APPLICATIONS OF
MODELLING AND SIMULATION
http://arqiipubl.com/ams eISSN 2600-8084 VOL 3, NO. 2, 2019, 85-94

Numerical Investigation of Hydrokinetic Savonius Rotor with Two Shielding Plates

M. Hemida[1], W. A. Abdel-Fadeel[2], A. Ramadan[3], and W. A. Aissa[2*]

[1]Ministry of Irrigation and Water Recourses, Souhag, Egypt
[2]Faculty of Energy Engineering, Aswan University, Aswan, Egypt
[3]Arab Academy for Science, Technology & Maritime Transport, Cairo, Egypt

[*]Corresponding author: waessa@energy.aswu.edu.eg

Received 10 February 2019, Revised 13 March 2019, Accepted 05 April 2019.

Abstract: Savonius hydrokinetic rotor is an evolution of the conventional savonius wind turbine. This rotor is suitable for low flow velocities with simple design, high starting torque and working for all flow directions. However, the torque fluctuation of this rotor is a serious problem due to the negative moment generated at the returning blade of this rotor. In this paper, a numerical investigation with commercial computational fluid dynamic (CFD) package FLUENT for modified savonius rotor with two deflector plates in the upstream of the turbine is conducted to find the optimum position of the two deflector plates to increase the power coefficient using water as a working medium. Results show that the model with the best orientation of the two deflector plates in the upstream increases the power coefficient by 80%. This may be due to the overlapped effect of decreasing the negative moment on the returning blade and the increased flow velocity at the advancing blade.

Keywords: Hydrokinetic; Numerical; Savonius rotor; Shielding plate.

1. INTRODUCTION

Tidal power is a form of renewable energy sources which resulted from the movement of the moon around the earth all the month. Utilisation of this renewable energy source necessitated searching for new techniques to harness this energy. Horizontal axis turbines are found to be the most appropriate drivers for the high speeds of water in oceans. In the last decades, the hydrokinetic energy of low speed flows in canals and rivers attracted more attention due to its availability and the constant intensity in some water channels around the year. Extracting this power from the water flow required searching for a new turbine which operates at low flow speeds with moderate changes in torque and rotation speed. Savonius rotor is found to be the most suitable turbine for this application. Savonius rotor is classified as a drag type, vertical axis rotor (Figure 1). It depends primarily on the difference between the drag force generated on the concave and the convex sides of the rotor. This difference creates the torque which rotates the rotor. This rotor works for all directions of flow without yawing system, and it does not need special manufacturing processes. Moreover, it has a high starting torque and low cost of fabrication.

On the other side, the low power coefficient of this rotor cannot be neglected. This low power coefficient resulted from the nature of the generated torque which resulted from the difference of the generated drag force between the concave side and the convex side. Due to the rotation of the rotor, the net averaged torque changes continuously and will fluctuate. This averaged torque may be enhanced by increasing the positive drag force acting on the advancing blade or decreasing the negative drag force acting on the returning blade. This improvement may be obtained by using deflector plates in the upstream of the turbine. Deflector plate at the returning blade will shield this part from the rotor from the main flow stream and decrease the inlet velocity and consequently the drag force at this part of the rotor will decrease. On the other hand, the deflector plate at the advancing blade will guide the main flow stream with gradual increase of flow velocity into this part of the rotor. This will increase the drag force at this part of the rotor. The net effect of the two deflector plates at the entrance increased the net average torque generated by the rotor. Using these deflector plates in hydrokinetic turbines would not make savonius rotor misses the advantage of operation in any flow direction because the flow in the river or canal will be unidirectional and the facility will be held to work in this direction.

The operation and design parameters of savonius rotors have been experimentally and numerically investigated to find the optimum operating conditions. Jaohindy *et al.* [1] developed a numerical model to investigate the effect of lift force on the performance of savonius rotor. They found that the effect of lift force appears in the range of tip speed ratios less than 0.6. Above this tip speed ratio, the lift force effect decreases and the effect of drag force increases.

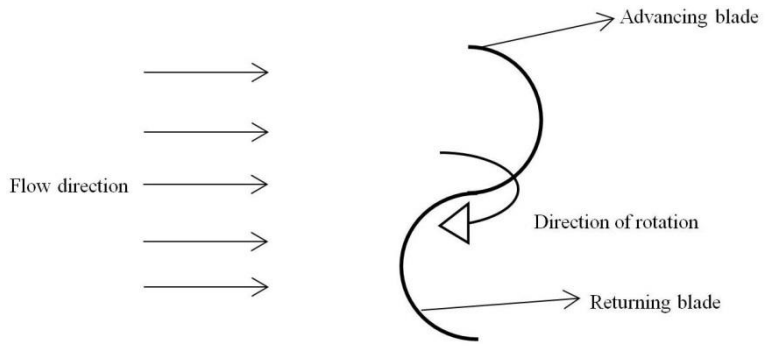

Figure 1. Savonius turbine's blade and flow direction

Hayashi *et al.* [2] investigated the performance of a single stage and three stages savonius rotor with and without guide vanes. They found that guide vanes increased the torque coefficient in the low tip speed ratio but decreased the coefficient in the high tip speed ratio. They also found that the three stage rotor without guide vanes has better torque characteristics than the one stage rotor with guide vanes for tip speed ratio larger than 0.8. Mahmoud *et al.* [3] investigated experimentally the effect of some design parameters on the performance of savonius wind turbine. They found that the two blades rotor is more efficient than three and four ones. The rotor with end plates gave higher efficiency than those of without end plates. Double stage rotors have higher performance compared to single stage rotors. The rotors without overlap ratio were better in operation than those with overlap. The results also showed that the power coefficient increases with raising the aspect ratio.

Modi *et al.* [4] investigated experimentally the effect of aspect ratio and overlap ratio on several single and two stage models to drive an irrigation pump. They found that the optimum value of aspect ratio is 0.77, absence of a gap between the blades resulted in maximum output, while the influence of overlap was particularly noticeable only for overlap to rotor diameter ratio that is greater than 0.22. Blackwell *et al.* [5] reported that the two-stage geometry has better aerodynamic performance than the three-stage one, with the exception of starting torque. It was also found that the increase in the aspect ratio improved the rotor performance. Ramadan *et al.* [6] developed a numerical model to compare between modified fullness savonius rotor, conventional two semicircular blades rotor and three blades rotor. They also experimentally investigated the performance of the three rotors in air as working medium. They found that the modified fullness savonius rotor has the highest power coefficient of 0.28 which is higher than the conventional two semicircular blade rotors (0.14) and three blade rotors (0.1).

Elbatran *et al.* [7] used a numerical model to investigate the effect of the duct with a nozzle at the entrance of ducted savonius water turbine on the performance. They compared the performance of conventional savonius rotor with six models with different ratios of outlet to inlet diameters of the nozzle. With Reynolds number, *Re* of 1.32×10^5, the water speed was increased using ducted nozzle savonius water turbine and power coefficient, C_p was increased by 78% when compared to the conventional savonius turbine. Moreover, the ducted nozzle shields the returning blade, thus reducing the reversing torque of the turbine. Kamoji *et al.* [8] investigated experimentally the effect of dimension parameters of the modified savonius rotor without a central shaft on the performance of the turbine. They found that the modified savonius rotor without central shaft with an overlap ratio of 0.0, blade arc angle of 124° and aspect ratio of 0.7 has a maximum C_p of 0.21 at *Re* of 1.5×10^5 which is higher than that of the conventional savonius turbine. They also developed a correlation for a single stage modified savonius rotor to predict the moment coefficient in terms of Reynolds number and tip speed ratio. El-Baz *et al.* [9] investigated the performance of a three-rotor savonius turbine using computational fluid dynamics (CFD). The results showed that the average moment coefficient and the power coefficient of the three-rotor turbine are higher than those of the single rotor turbine. At the tip speed ratio of 1.2, the three-rotor turbine moment and power are 44% higher than the values which obtained from the single rotor turbine. Mohamed [10] used CFD to investigate the effect of the number of blades on the performance of the savonius turbine. Further, the effect of an obstacle shielding the returning blade was studied and it was found that a two-blade rotor was better than the three-blade design. A considerable improvement of the performance of savonius turbines by using an obstacle shielding the returning blade by more than 27% than conventional savonius rotor was obtained. Golecha *et al.* [11] studied experimentally the effect of deflector plate position on the performance of modified savonius water turbine at *Re* 1.32×10^5 and the effect of the deflector plate on the two stages and three stage modified savonius rotors. They found that power coefficient increased by 50% with deflector plate placed at its optimal position for single stage modified savonius rotor and power coefficient increased by 42%, 31% and 17% with deflector plate for two-stage 0° phase shift, 90° phase shift and three stages modified savonius rotor respectively.

Golecha *et al.* [12] studied experimentally the effect of two deflectors position, one on the advancing blade and the other on the returning blade on the performance of modified savonius rotor at *Re* 1.32×10^5 in water as working fluid. They found that the two deflectors at the entrance of the turbine placed at their optimum position

increased the power coefficient to 0.35 at tip speed ratio of 1.08. Iio *et al.* [13] investigated experimentally the effect of one shielding plate on the performance of horizontal axis savonius rotor and the distance between the rotor and the bottom wall of the tunnel which was expressed in a non-dimensional form. They found that the maximum power coefficient obtained with the shielding plate is 0.47 which was higher than the rotor without shielding plate by 80%. Moreover, they found that the best clearance ratio is 0.73. Talukdar *et al.* [14] compared experimentally between two semicircular blades, three semicircular blades, and elliptical blade and the effect of immersion level on the performance of the three blades in water as working fluid. They found that the maximum power coefficient of the two semicircular blades is higher than that of the elliptical blade and the three semicircular blades by 28.6% and 39.2% respectively. Moreover, they found that the performance decreased by decreasing immersion level for the three turbines.

From the described researches, blade profile, flow speed and angular velocity of rotor are the most important parameters which control the rotor performance in terms of power coefficient and torque coefficient. The drag force changes linearly with the squared flow velocity. Therefore, the drag forces increase with the increasing flow velocity, and thus increased fluctuations in high flow velocities. This makes the savonius rotor to be the most appropriate driver in the low speed water flow which ranges from 0.5 m/s to 1.5 m/s in canals and rivers. The main objective of this study is to investigate numerically the performance of savonius rotor which was developed by Mohamed [10] in air as working fluid with two guiding plates at the entrance of the rotor and to find the best orientation of these plates by increasing the inlet flow velocity and decreasing the negative torque acting on the returning blade.

2. EFFECT OF DEFLECTOR PLATE AND OBSTACLE PLATE

The main goal of the two guiding plates at the entrance of the turbine (Figure 2) is to improve the performance of the rotor. This improvement is obtained by:

a) Increasing the positive forces acting on the advancing blade by increasing the flow velocity at the entrance of this blade which will increase the positive moment of the rotor.
b) Decreasing the negative forces acting on the returning blade by shielding the flow from the returning blade. Thus, the negative moment acts in the adverse direction of rotation will decrease.

In the present research, the numerical model is performed to investigate the performance of the savonius rotor obtained by Mohamed [10] with and without deflector plates in the upstream of water flow. The blade is divided into two fixed points at the start and the end (P_4, P_5) and three movable points (P_1, P_2, P_3) as shown in Figure 3. Using numerical models, the performance of this rotor was investigated with and without deflector plates using air as a working fluid, and the following results for the optimum performance was reported:

$X_{P1}/r = 0.54822,\ Y_{P1}/r = 0.19762, X_{P2}/r = 0.34849, Y_{P2}/r = -0.37885, X_{P3}/r = -0.54593, Y_{P3}/r = -0.770346,$
$X_{d1}/d = -0.41882,\ \ Y_{d1}/d = 1.24505, X_{d2}/d = -0.3433, Y_{d2}/d = 2.29074, X_{o1}/d = -1.2828,\ Y_{o1}/d = -0.4037$
$X_{o2}/d = -1.27654,\ Y_{o2}/d = -1.16339$

$a/d = -0.00635,\ e/d = 0.18286$, length of deflector plate $l_d/d = 1.048$, length of obstacle plate $l_o/d = 0.7597$.

Descriptions of symbols used in this paper are shown in the Appendix. In the present research, two parameters are modified in rotor design:

- Overlap ratio = 0.
- No rotating shaft between the two end plates.

The best orientation of the two deflector plates is obtained by investigating the performance of the rotor without deflector plates at different tip speed ratios. The rotor with the highest power coefficient at specific tip speed ratio will be investigated at this tip speed ratio by placing the obstacle plate only at the entrance of the returning plate. The Cartesian coordinates of this plate are shown in Figure 2 measured from the center of rotation of the rotor. The coordinate of point *A* and the length of the obstacle plate will be fixed and this plate will be rotated around point *A* in clockwise and counterclockwise directions to get the best angle of the obstacle θ. With this position of the obstacle plate, the deflector plate will be inspected by fixing point *B* coordinate and the length of the deflector plate and rotating the plate in clockwise and counterclockwise directions around point *B* to get the best angle of the deflector φ. Finally, the rotor with the two plates positioned at their optimum orientation will be examined at different tip speed ratios to obtain the best operating conditions of the rotor.

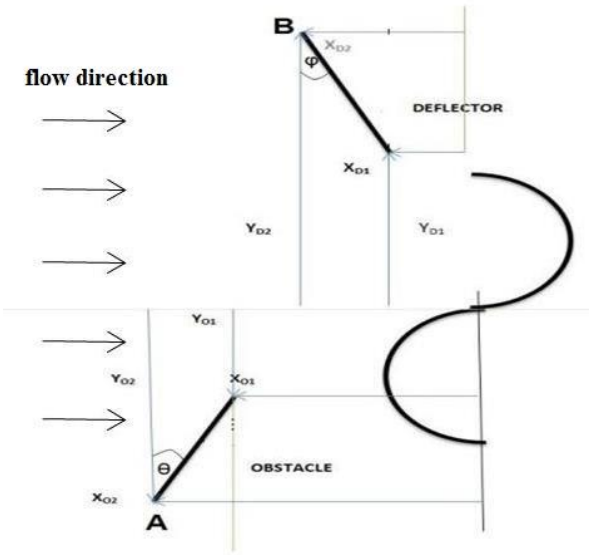

Figure 2. Savonius rotor with two deflector plates at the entrance

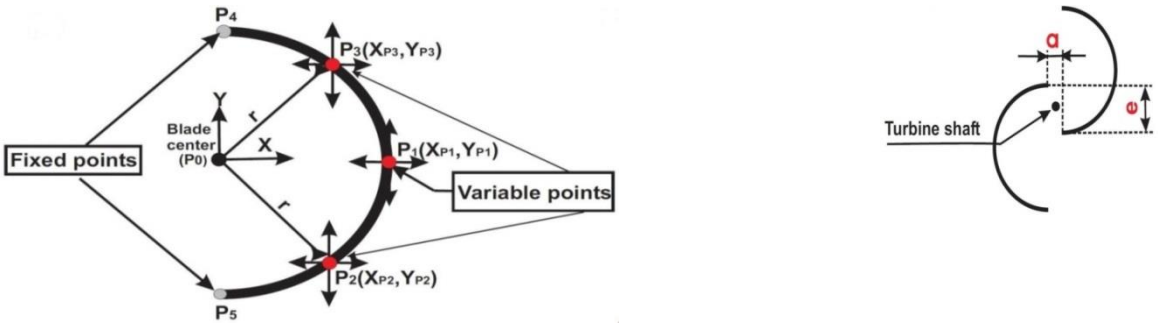

Figure 3. Mohamed's profile for the modified savonius turbine

3. NUMERICAL ANALYSIS

In the present work, FLUENT commercial software is used as CFD program to simulate the savonius rotor. FLUENT is a CFD software using the finite element method to solve the flow problems in or around complex geometries. In the FLUENT program, physical properties of the flow are specified and analysis technique and turbulence model are chosen. It is found that the two-dimensional analysis has a suitable accuracy, and can be used to conduct the numerical analysis in a shorter time. Gambit is a software program which is used to generate the mesh of the required domains which is exported to FLUENT program for the numerical analysis. Quad/tri pave scheme is used for mesh generation of the model.

The overall domain is divided into two subdomains to facilitate simulation of the rotor rotation. The highest resolution subdomain contains the grid elements surrounding the rotor (referred to as the rotating domain). The lowest resolution subdomain is the outer domain (referred to as the stationary domain). As shown in Figure 4, dimensions of the stationary domain were chosen to be large to minimise blockage effect without increasing computing time [15] and the diameter of the rotating domain is $1.2D$ where D is a blade diameter. Sliding mesh model is applied to obtain the rotating motion of the turbine. The enhanced wall function method is applied to ensure the precise resolution of the boundary layer prediction [9]. The wall function approach requires the dimensionless distance of the first grid point from the wall ($y+$) to be greater than 30, which is used in the present work.

3.1 Governing Equations

In the present study, the realisable k-ε model was used for the analysis. The standard k-ε model is improved by using variable C_μ for computing the turbulent viscosity instead of the constant value in the standard k-ε model and this provides superior performance for flows involving rotation, boundary layers under strong adverse pressure gradients, separation, and recirculation [16]. Every simulation takes ten revolutions to allow for a convergence state. The results of the last revolution are used for the analysis. The convergence criterion was determined by neglecting all residuals which are below 10^{-5}. The SIMPLE (Semi-Implicit Method for Pressure-Linked Equations) pressure-velocity coupling method is used in all simulations. A second order upwind spatial

discretisation scheme is used for the equations of momentum, turbulent kinetic energy, pressure, and turbulent dissipation rate and a least squares cell-based scheme is used for the gradients

Simulations are carried out with varying tip speed ratio values to obtain the values of torque coefficient and power coefficient at different angular velocities. The tip speed ratio is the blade tip speed divided by the flow speed and may be expressed in the form:

$$TSR = \lambda = \frac{\omega r}{V} \tag{1}$$

where ω is the angular velocity of the rotor, r is turbine radius and V is the uniform flow velocity. Power coefficient represents the harnessed power from the available flow power and may be expressed in the form:

$$C_P = \frac{T\omega}{0.5\rho A V^3} \tag{2}$$

where $A = DH$ is the projected area of the turbine and T is the average torque of the turbine. Torque coefficient of the turbine may be expressed as:

$$C_T = \frac{T}{0.5\rho A r V^2} \tag{3}$$

where ρ is the water density

The relation between the power coefficient and torque coefficient is:

$$C_P = \lambda C_T \tag{4}$$

The analysis is performed using a turbine diameter of 0.245 m and *Re* equals 1.32×10^5. The height of the turbine is taken as 0.17 m in the transverse direction of the turbine. The length of the obstacle plate and deflector plate are 7.597 cm and 10.48 cm respectively. The initial rotor angle of the rotor is zero degree measured from the vertical axis, so that the rotor axis is perpendicular to the flow direction. As shown in Figure 5 the torque coefficient is obtained from CFD analysis which calculates the net torque from the drag force difference between the concave side and the convex side. Torque coefficient value changes with flow time so that for every tip speed ratio, performance analysis is done to get the value of torque coefficient. The value of torque coefficient at every time step is integrated over the projected area of the rotor A and averaged overflow time. Every torque coefficient is multiplied by tip speed ratio to get power coefficient at every tip speed ratio.

Figure 6 illustrates the effect of the number of cells on the performance of the rotor at tip speed equals 0.7 on basis of torque coefficient. The number of cells ranged from 80,000 to 147,000. The torque coefficient is getting stable and constant after 130,000 cells and whatever the increase in a number of cells. Moreover, the time step size is considered as in El-Baz *et al.* [9].

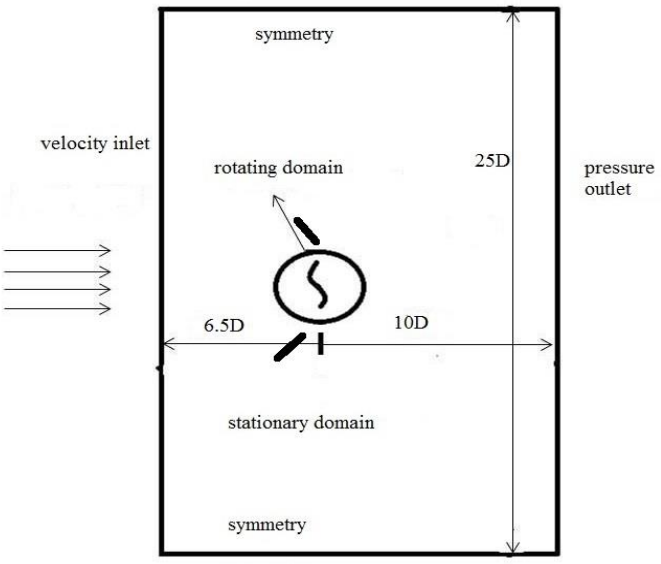

Figure 4. Computing domains and boundary conditions

3.2 Model Validation

Model is validated by comparing the obtained experimental results from Golecha *et al.* [11] with the results obtained from the numerical model with the configuration of Kamoji *et al.* [8]. Figure 7 shows the variation of torque coefficient with tip speed ratio for numerical investigation which seems to be in a good agreement with the experimental research. The maximum error value is 10% and the average error value is 4.8%.

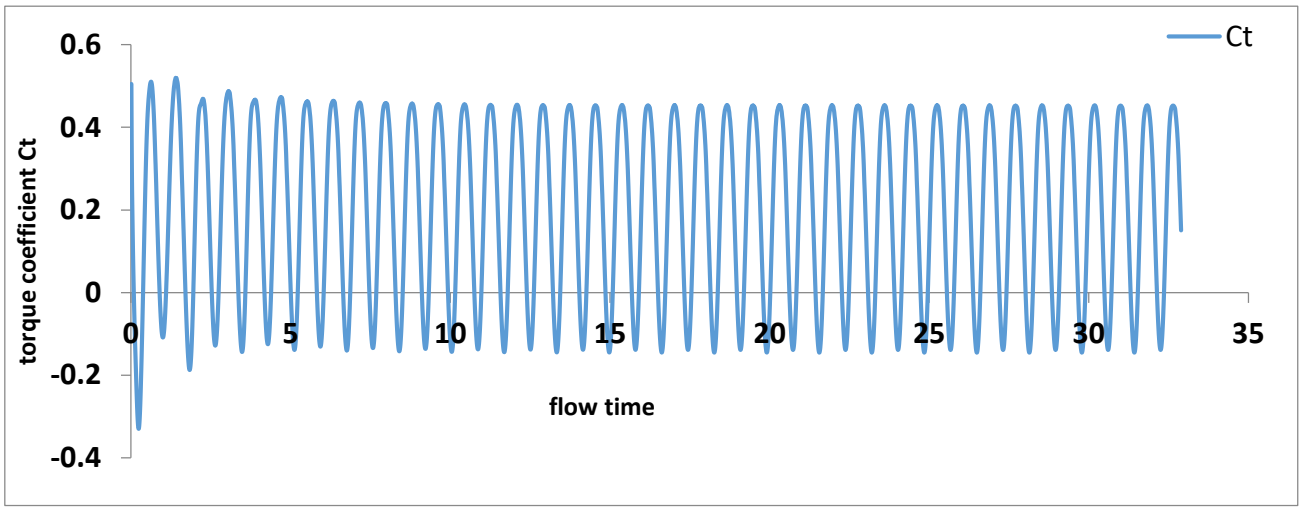

Figure 5. Change of torque coefficient obtained from ANSYS fluent with flow time at tip speed ratio = 0.6

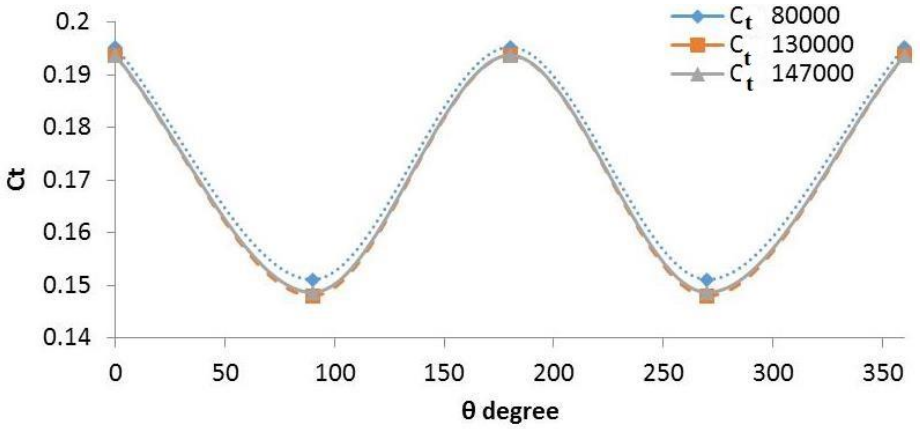

Figure 6. Grid independence test

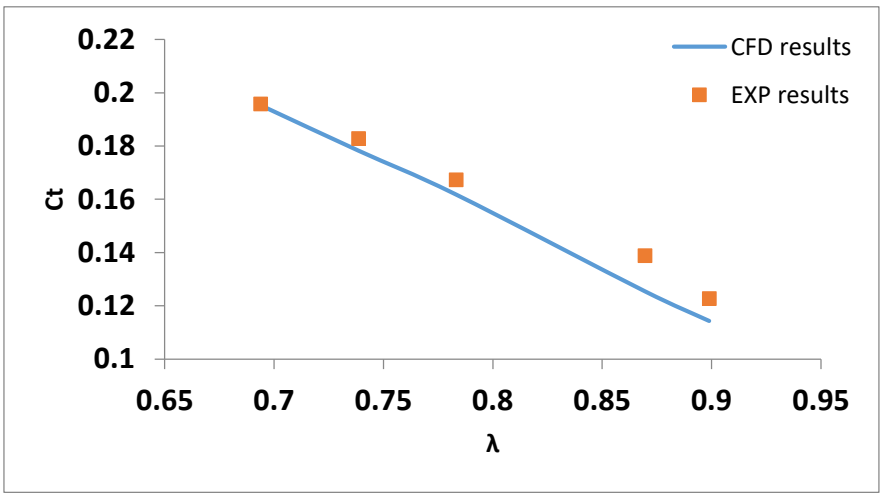

Figure 7. The torque coefficient validation

4. RESULTS AND DISCUSSION

As shown in Figure 8, the magnitude of the angle θ is 10° in clockwise direction and for angle φ is 5° in counterclockwise direction for the best orientation of the two deflector plates. The obstacle plate is placed firstly and rotated around point *A*. Step angle was taken as 5° in clockwise and counterclockwise directions. Power coefficient at each step is obtained and plotted versus angle θ at tip speed ratio 0.6. The maximum power coefficient obtained at an obstacle angle 10° in clockwise direction. The rotor with this obstacle plate angle is inspected by adding deflector plate which rotated around point *B* to find the best deflector plate angle φ with the same procedure followed for obstacle plate. The best deflector plate angle is 5° in the counterclockwise direction at tip speed ratio 0.6

Figures 9 and 10 show pressure distribution along the upstream and downstream of rotor without deflectors and rotor with deflectors respectively. The difference between the upstream pressure and downstream pressure represents the harnessed power by the turbine and the area between the lines represents the pressure difference which converted into mechanical power by the turbine. The fluctuation of the upstream pressure at the lower half of the turbine and the downstream pressure at the upper half of the turbine may be noticed. This fluctuation for the rotor with deflectors is less than that of the rotor without deflectors. Moreover, the downstream pressure at the upper half of the turbine with deflectors is more uniform than the turbine without deflectors. This may be due to the flow concentration effect of the two deflector plates at the entrance of the turbine. On the other hand, the back pressure effect on the lower tip of the two cases is noticed in Figures 9 and 10. This back pressure may be considered as lost power because it affects in the adverse direction of the mean flow and this minimises the net averaged torque from the turbine.

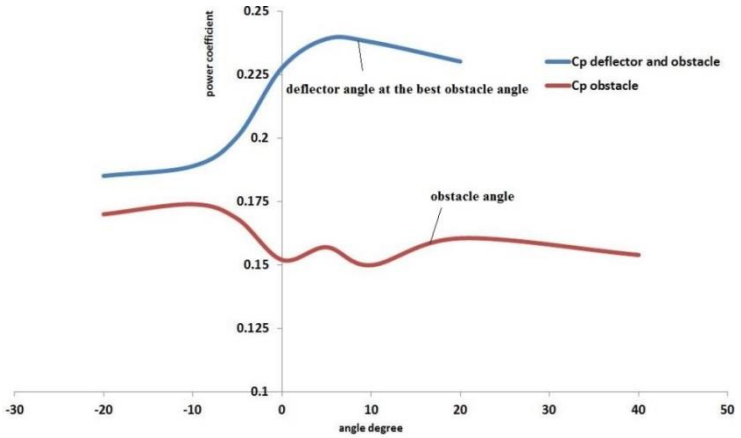

Figure 8. Power coefficient variation with obstacle angle only and deflector angle combined with best obstacle angle

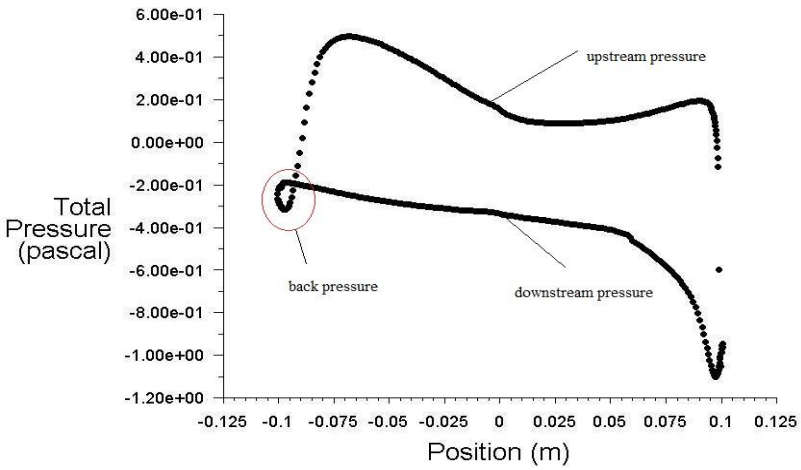

Figure 9. Pressure distribution on the upstream and downstream of the turbine without deflectors

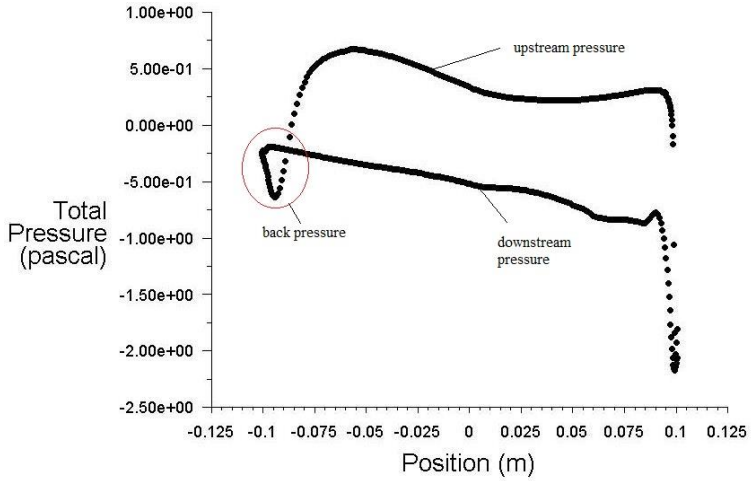

Figure 10. Pressure distribution on the upstream and downstream of the turbine with deflectors

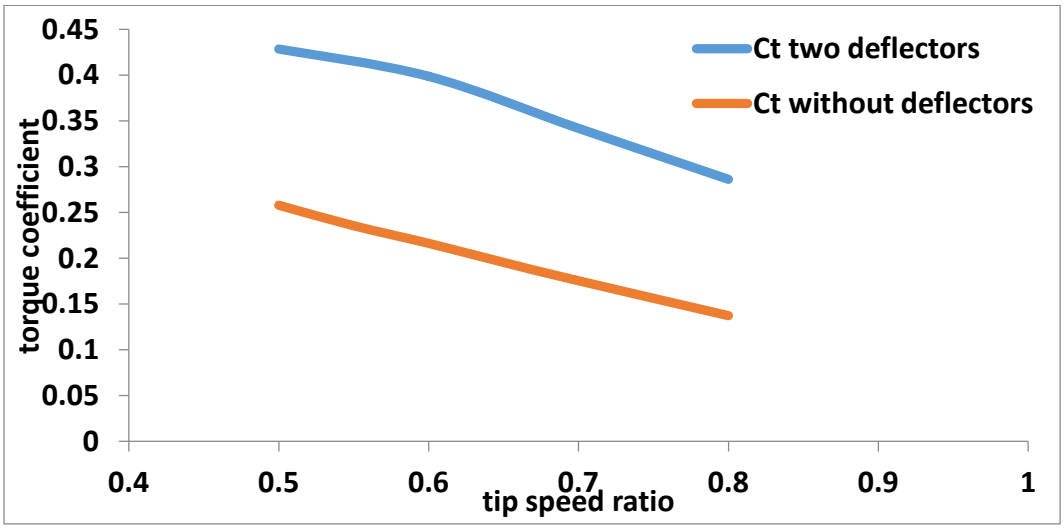

Figure 11. Torque coefficient variation with different tip speed ratios for the rotor with and without deflectors

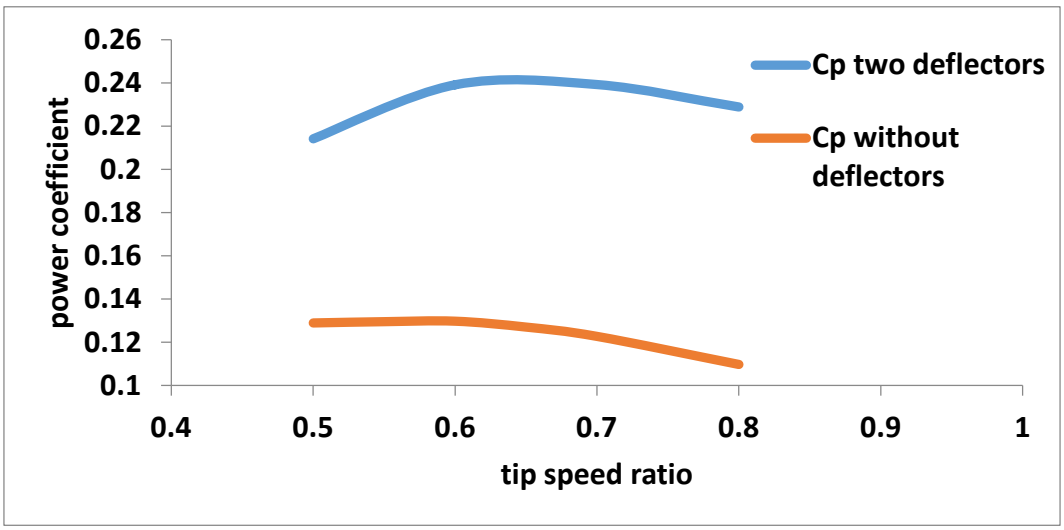

Figure 12. Power coefficient variation with different tip speed ratios for the rotor with and without deflectors

Figure 11 shows the variation of the torque coefficient of the turbine with and without shielding plates and the tip speed ratio. It is obvious that a torque performance characteristic of the turbine with two deflectors is higher than that of the turbine without deflectors. Power coefficient variation with tip speed ratio is shown in Figure 12. The maximum power coefficient of the turbine without deflectors is 0.13 at a tip speed ratio of 0.6 and for the turbine with two deflectors is 0.24 at tip speed ratio 0.7 with 84% increase of power coefficient. This may be due to the uniform pressure distribution on the upstream and the downstream of the turbine with the deflector plates.

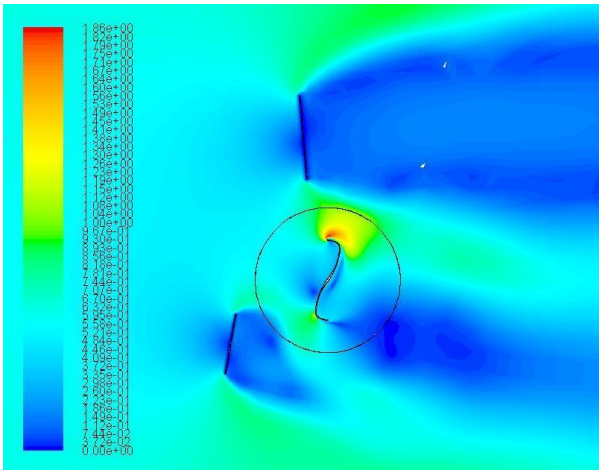

Figure 13. Velocity contours around the rotor at tip speed ratio 0.7

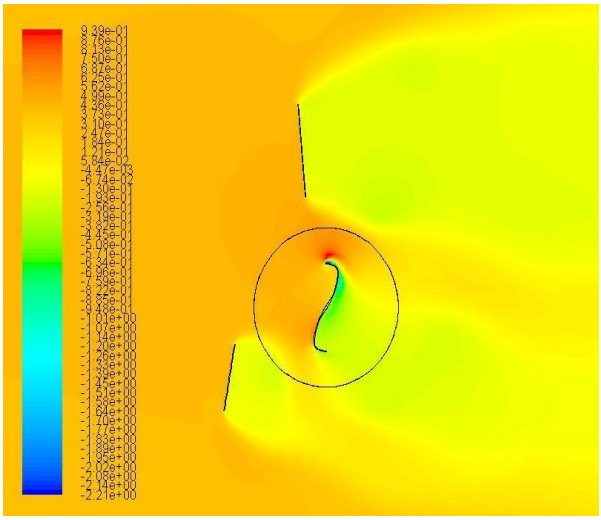

Figure 14. Pressure contours around the rotor at tip speed ratio 0.7

Figures 13 and 14 show the velocity contours and pressure contours respectively around the rotor with deflector plates at the entrance. As shown in Figure 13, two vortices only formed (the dark blue regions) around the rotor with small intensities. The first one at the upstream and the other at the downstream. These vortices are considered as lost power from the water flow and cause pressure drop along the blade diameter at the upstream and the downstream. This pressure drop decreases the harnessed power by the rotor from the water flow. This is shown in Figure 14 which indicates the pressure contours around the blade diameter. The pressure along the upstream (the yellowish brown region) and the downstream (the light green region) is more uniform and gradually stratified from the lower half of the rotor to the upper half of the rotor. The front of uniform pressure region (light brown region) is formed from the lower half of the upper plate to the lower half of the rotor. This front creates a new field of high speed regions that indicated in the velocity contours (Figure 13) at the upstream of the rotor (the light blue region) which show increase in velocity at the upper tip and the lower tip of the rotor (green regions in velocity contours) and eliminates the formation of vortices at these critical regions around the rotor.

5. CONCLUSION

The present work investigates the performance of the blade profile obtained by Mohamed for the hydrokinetic turbine with and without deflector plates. This model is solved numerically by the commercial finite volume solver ANSYS-FLUENT to get the torque coefficient and the power coefficient of the turbine blade. The numerical analysis indicates that the rotor with two deflector plates at the entrance of the turbine has the maximum C_p of 24% for tip speed ratio of 0.7 and streamflow velocity of 0.6 m/s which is higher than the rotor without deflector plates by 84%. A uniform pressure distribution on the upstream and downstream of the turbine may be considered as the reason for this improvement due to the concentration of flow by the deflector plates which minimise the vortices formation around the rotor by accelerating the flow into the turbine. The acceleration effect decreases the act of pressure drop at the upstream of the rotor which is responsible for vortices formation at some regions and decreasing the net averaged torque of the rotor.

REFERENCES

[1] P. Jaohindy, S. McTavish, F. Garde and A. Bastide, An analysis of the transient forces acting on savonius rotors with different aspect ratios, *Renewable Energy*, 55, 286-295, 2013.

[2] T. Hayashi, L. Yan and H. Yutaka, Wind tunnel tests on a different phase three-stage savonius rotor, *JSME International Journal Series B Fluids and Thermal Engineering*, 48(1), 9-16, 2005.

[3] N. Mahmoud, A. El-Haroun, E. Wahba and M. Nasef, An experimental study on improvement of savonius rotor performance, *Alexandria Engineering Journal*, 51, 19-25, 2012.

[4] V. Modi, N. Roth and M. Fernando, Optimum-configuration studies and prototype design of a wind-energy-operated irrigation system, *Journal of Wind Engineering and Industrial Aerodynamics*, 16, 85-96, 1984.

[5] B. Blackwell, R. Sheldahl and L. Feltz, *Wind Tunnel Performance Data for Two and Three-bucket Savonius Rotors*. Albuquerque, NM: Sandia Labs, 1977.

[6] A. Ramadan, K. Yousef, M. Said and M. H. Mohamed, Shape optimization and experimental validation of a drag vertical axis wind turbine, *Energy*, 151, 839-853, 2018.

[7] A. H. Elbatran, M. Ahmed Yasser and S. Shehata Ahmed, Performance study of ducted nozzle savonius water turbine, comparison with conventional savonius turbine, *Energy*, 134, 566-584, 2017.

[8] M. A. Kamoji, B. Kedare Shireesh and S. V. Prabhu, Experimental investigations on single stage modified savonius rotor, *Applied Energy*, 86(7), 1064-1073, 2009.

[9] A. R. El-Baz, K. Youssef and M. H. Mohamed, Innovative improvement of a drag wind turbine performance, *Renewable Energy*, 86, 89-98, 2016.

[10] M. H. Mohamed, Design Optimization of Savonius and Wells Turbines. Ottovon-Guericke University Magdeburg, 2011.

[11] K. Golecha, T. I. Eldho and S. V. Prabhu, Influence of the deflector plate on the performance of modified savonius water turbine, *Applied Energy*, 88(9), 3207-3217, 2011.

[12] K. Golecha, T. I. Eldho and S. V. Prabhu. Performance study of modified Savonius water turbine with two deflector plates, *International Journal of Rotating Machinery*, 2012, ID 679247.

[13] Iio Shouichiro, Katayama Yusuke, Uchiyama Fuminori, Sato Eiichi and Ikeda Toshihiko, Influence of setting condition on characteristics of savonius hydraulic turbine with a shield plate, *Journal of Thermal Science*, 20(3), 224-228, 2011.

[14] P. Talukdar, A. Sardar, V. Kulkarni and U. Saha, Parametric analysis of model savonius hydrokinetic turbines through experimental and computational investigations, *Energy Conversion and Management*, 158, 36-49, 2018.

[15] A. Ramadan, Innovative design investigation of an augmented drag vertical Axis wind turbine under unsteady characteristics, *Proceedings of the 4th International Conference and Exhibition on Mechanical and Aerospace Engineering*, Orlando, USA, 2016, pp. 1-19.

[16] ANSYS, *14.0 User's Guide*, ANSYS Inc., 2011.

APPENDIX

Nomenclature

A	The projected area of the turbine
C_p	The power coefficient
C_T	The torque coefficient
D	The blade diameter
R	The rotor radius
Re	Reynolds number
T	The average torque
V	The approaching water speed

Greek Letters

ρ	The density of the water
ω	The angular speed of the rotor
υ	Kinematic viscosity
λ	The tip speed ratio of the turbine